

A developmental arc of white matter supporting a growing diversity of brain dynamics

Evelyn Tang,¹ Chad Giusti,¹ Graham Baum,² Shi Gu,¹ Eli Pollock,³ Ari E. Kahn,¹ David Roalf,² Tyler M. Moore,² Kosha Ruparel,² Ruben C. Gur,² Raquel E. Gur,² Theodore D. Satterthwaite,^{2,4} and Danielle S. Bassett^{1,5,4}

¹Department of Bioengineering, University of Pennsylvania, PA 19104

²Brain Behavior Laboratory, Department of Psychiatry, University of Pennsylvania, PA 19104

³Department of Physics, University of Pennsylvania, PA 19104

⁴These authors contributed equally.

⁵Department of Electrical and Systems Engineering, University of Pennsylvania, PA 19104

(Dated: October, 2016)

As the human brain develops, it increasingly supports the coordinated synchronization and control of neural activity. The mechanism by which white matter evolves to support this coordination is not well understood. We use a network representation of diffusion imaging data to show that white matter connectivity becomes increasingly optimized for a diverse range of predicted dynamics in development. Such optimized topologies emerge across 882 youth from ages 8 to 22 evidencing increasing local specialization. Notably, stable controllers in subcortical areas are negatively related to cognitive performance. Seeking to investigate structural mechanisms that support these changes, we simulate network evolution with a set of growth rules, to find that all brain networks – from child to adult – are structured in a manner highly optimized for network control. We further observe differences in the predicted control mechanisms of the child and adult brains, suggesting that the white matter architecture in children has a greater potential to increasingly support brain state transitions, potentially underlying cognitive switching. This work suggests mechanisms for the propagation and stabilization of brain activity at various spatial scales, revealing a possible mechanism of human brain development that preferentially optimizes dynamic network control over static features of network architecture.

INTRODUCTION

Modern neuroimaging techniques reveal the organization of the brain’s white matter microstructure [1], which forms a large-scale wiring diagram or *connectome* [2] thought to support the brain’s diverse dynamics [3]. Importantly, this architecture changes as children mature into adults, potentially facilitating the emergence of adult cognitive function [4, 5]. Despite the intuitive relationship between network structure and brain function, fundamental mechanistic theories explaining the development of white matter organization and its relationship to emerging cognition in humans have remained elusive. Such a theory would have far-reaching implications for our understanding of normative cognitive development as well as vulnerabilities to neuropsychiatric disorders.

Here we investigate how structural connectivity facilitates changes and constrains patterns of dynamics in the developing brain. Drawing from theoretical physics and engineering, we study two structural predictors of brain dynamics – controllability [6–8] and synchronizability [9]. We use these two notions to examine how brains might be optimized for different types of dynamics, and whether individual brains are optimized differently. Controllability is a structural predictor of the ease of switching from one dynamical state to another [10], a capability that is critical for traversing a broad state space encompassing a diverse dynamic repertoire [11]. Synchronizability is a structural predictor of the ability for regions in the network to support the same temporal dynamical pattern [12], a phenomenon that can facilitate inter-regional

communication when implemented locally [13, 14] but can facilitate pathological seizure-like dynamics when implemented globally [15, 16]. We hypothesize that white matter networks develop from childhood to adulthood explicitly to maximize controllability and reduce synchronizability.

To test this hypothesis, we examine controllability and synchronizability in structural brain networks derived from diffusion tensor imaging data, which we have represented as weighted adjacency matrices (Fig. 1a; see Methods). We determine the relationship between controllability and synchronizability in a sample of 882 youth from the ages of 8 to 22, and demonstrate that networks become optimized for diverse dynamics as children develop, following trajectories that depend on predicted oscillatory modes with different spatial extents. Further, we provide supporting evidence for the hypothesis that a balance of controllability across brain regions is required for optimal cognitive function.

To better understand potential mechanisms of these trajectories, we build an evolutionary model that describes the observed increase in mean controllability and decrease in synchronizability with age. By exploring changes between networks with similar connection strengths but different connection topologies, we explore the extent to which brain networks are optimized for these architectural features. Then, we define a given subject’s capacity to alter its topology towards increasingly diverse dynamics by extracting parameters that govern the speed, extent and fall-off of network optimization. These novel statistics allow us to assess whether chil-

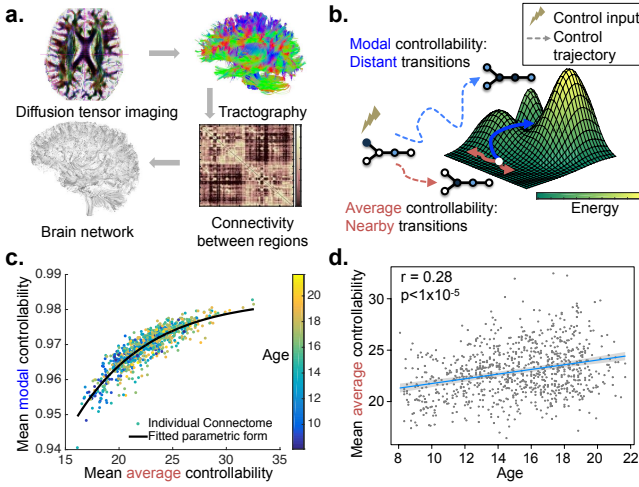


Figure 1: The developmental arc of controllability in brain networks **a.** Diffusion tensor imaging measures the direction of water diffusion in the brain. From this data, white matter streamlines can be reconstructed that connect brain regions in a structural network. **b.** Average controllability: structural support for moving the brain to easy-to-reach states; mean modal controllability: structural support for moving the brain to difficult-to-reach states. **c.** We examine 882 healthy individuals from the ages of 8 to 22, where each circle represents controllability metrics calculated on the brain network of a single individual. The color bar denotes the age of the subjects, illustrating a significant correlation between age and both average and modal controllability. We fit this clear developmental arc, with an exponential form $y = a + b \exp(cx)$, where x is mean average controllability and y is mean modal controllability calculated on each brain network. Parameters for best fit curve: $a = 0.98$, $b = -0.35$ and $c = -0.14$. **d.** Mean average controllability significantly increases with age: Pearson’s correlation coefficient $r = 0.28$, $df = 881$, $p < 1 \times 10^{-5}$, controlled for brain volume, head motion, sex, and handedness. Blue lines shows best linear fit; gray envelope denotes 95% confidence interval.

dren’s brains have greater potential for increasing their ability to move from one mental state to another (controllability). Finally, we demonstrate that the evolutionary rule based on controllability and synchronizability is a better fit to the observed empirical data than alternative rules constructed from traditional graph statistics (see Supplement).

RESULTS

The developmental arc: increasing controllability

We begin by asking “Do regions of the brain display different predispositions for controllability?” To answer this question, we examine two types of controllability, which describe the predicted ability to move the network into different states defined as patterns of regional ac-

tivity (Fig. 1b). *Average controllability* is a structural phenotype predicted to facilitate small changes in brain state, nearby on an energy landscape. In contrast, *modal controllability* is a structural phenotype predicted to facilitate large changes in brain state, distant on an energy landscape (see Methods).

To address whether there are related individual differences in types of controllability, we study these metrics in a cohort of 882 youth from ages 8 to 22 (see Supplement). We find that individuals whose brains display high mean average controllability also display high mean modal controllability (Pearson’s correlation coefficient $r = 0.87$, $df = 881$, $p < 1 \times 10^{-5}$; Fig. 1c). This suggests that brain networks that can support switches among nearby states can also support dynamical transitions among distant states. Further, we observe that average controllability increases as children age (Pearson correlation coefficient $r = 0.28$, $df = 881$, $p < 1 \times 10^{-5}$; Fig. 1d), as does modal controllability ($r = 0.22$, $df = 881$, $p < 1 \times 10^{-5}$, controlled for brain volume, head motion, sex and handedness). This developmental arc can be fit parsimoniously with the exponential equation $y = a + b \exp(cx)$ (see Methods).

Decreasing synchronizability

While controllability predicts the ability of a network to change between states, synchronizability predicts the ability of a network to persist in a single (synchronous) state. Mathematically, this property of a complex system can be studied using the master stability function [9, 17]. Specifically, stability under perturbations exists when this function is negative for all positive eigenvalues of the graph Laplacian $\{\lambda_i\}$, $i = 1, \dots, (N - 1)$, or – put another way – when all $\{\lambda_i\}$ fall within the region of stability (Fig. 2a). A larger spread of Laplacian eigenvalues will make the system more difficult to synchronize, and therefore an intuitive measure of global synchronizability is the inverse variance $1/\sigma^2(\{\lambda_i\})$ [18] (see Methods).

Using this theoretical scaffold, we observe that brain networks that are more synchronizable tend to display lower average controllability (Pearson’s correlation coefficient $r = -0.85$, $df = 881$, $p < 1 \times 10^{-5}$; Fig. 2b) as well as lower modal controllability ($r = -0.82$, $df = 881$, $p < 1 \times 10^{-5}$). While no known relationship between synchronizability and controllability exists, the correlation is intuitive in that it suggests that individuals who are theoretically predicted to more easily transition into a variety of dynamical states are less susceptible to having many regions locked in synchrony. Interestingly, the relationship between synchronizability and controllability is partially explained by age: synchronizability decreases as children age ($r = -0.37$, $df = 881$, $p < 1 \times 10^{-5}$; controlled for brain volume, head motion, sex and handedness; inset of Fig. 2b). This developmental arc can be

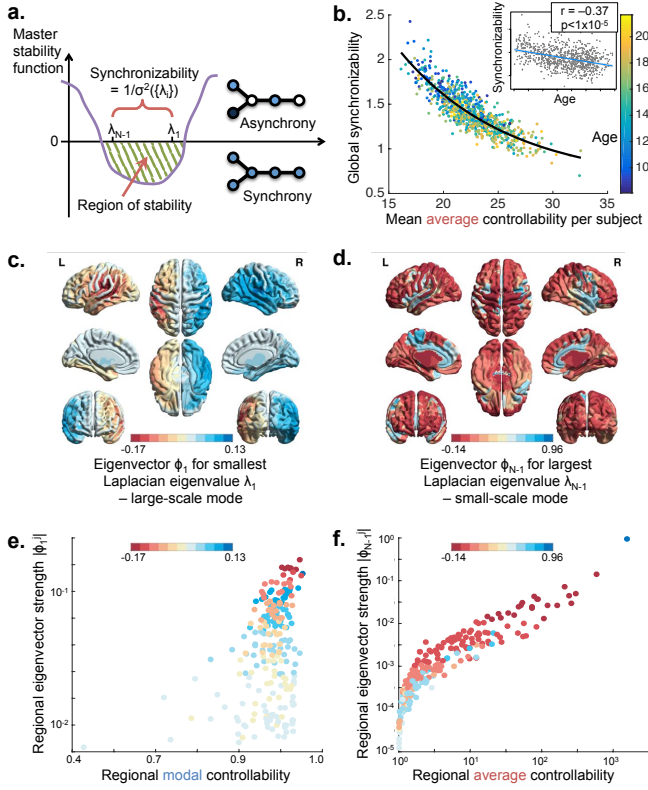


Figure 2: Synchronizability and the spatial extent of predicted oscillatory modes. (a) A synchronous state is operationalized as a state in which all nodes have the same activity magnitude. Such a state is stable when the master stability function is negative for all positive eigenvalues of the graph Laplacian (see Methods). We use the inverse spread of the Laplacian eigenvalues $1/\sigma^2(\{\lambda_i\})$ as a measure of global synchronizability. (b) Global synchronizability is anti-correlated with mean average controllability. The color bar and inset illustrates the significant correlation between age and synchronizability ($r = -0.37$, $df = 881$, $p < 1 \times 10^{-5}$; controlled for brain volume, head motion, sex and handedness). We fit this second developmental arc using the same exponential form, where now y is synchronizability and x remains the mean average controllability. Parameters for the best fit curve: $a = 0.62$, $b = 7.4$ and $c = -0.10$. (c) Spatial distribution of the eigenvector ϕ_1 for the smallest Laplacian eigenvalue λ_1 , showing which regions on a group-averaged network most strongly contribute to this large-scale mode. (d) Spatial distribution of the eigenvector ϕ_{N-1} for the largest Laplacian eigenvalue λ_{N-1} , showing which regions most strongly contribute to this small-scale mode. (e) Regions most relevant for this large-scale mode $|\phi_1^j|$ are positively correlated with regions of high modal controllability: $\rho = 0.27$, $df = 233$, $p < 1 \times 10^{-4}$. (f) Regions most relevant for this small-scale mode $|\phi_{N-1}^j|$ are positively correlated with regions of high average controllability: $r = 0.90$, $df = 233$, $p < 1 \times 10^{-5}$.

fit with an exponential form similar to that used to fit the arc of modal *versus* average controllability (see previous section). These results suggest that as the brain ma-

tures, its network architecture supports a larger range of dynamics (from nearby to distant states), and is less able to support globally synchronized states.

Spatial scales of oscillatory modes

In addition to providing intuitions regarding the network’s controllability, the structure of the graph Laplacian also provides information regarding the most likely modes of oscillatory dynamics in the system. An oscillatory mode is defined intuitively as the vibrational state of an oscillating system in which the frequency of vibration is the same for all elements. Mathematically, this concept is operationalized in the eigenvectors of the graph Laplacian. For example, the eigenvector ϕ_1 of the smallest positive Laplacian eigenvalue λ_1 is an odd mode, and the regional strength $|\phi_1^j|$ reflects its relative contribution [16] to large-scale oscillations [9] (Fig. 2c). By contrast, the eigenvector ϕ_{N-1} of the largest Laplacian eigenvalue λ_{N-1} is an even mode, and the regional strength $|\phi_{N-1}^j|$ reflects its relative contribution to small-scale oscillations (Fig. 2d).

We observe that the oscillatory modes of a network can be understood in terms of the network’s predisposition to various types of control. First, we observe that the regional strength of the large-scale oscillations $|\phi_1^j|$ is positively correlated with regional modal controllability (Spearman correlation coefficient $r = 0.27$, $df = 233$, $p < 1 \times 10^{-4}$; Fig. 2e), suggesting that regions that participate in synchronous behavior over long distances are also predicted to be good at moving the brain to distant states. Second, we observe that the regional strength of the small-scale oscillations $|\phi_{N-1}^j|$ is positively correlated with regional average controllability (Pearson’s correlation coefficient $r = 0.90$, $df = 233$, $p < 1 \times 10^{-5}$; Fig. 2f), suggesting that regions that participate in synchronous behavior over short distances are also predicted to be good at moving the brain to nearby states.

Super controllers and cognition

Given the global trends of increasing controllability and decreasing synchronizability with age, it is worth asking whether specific regions of the brain are driving these changes, or whether all regions contribute equally. Surprisingly, we observe that the regions that display the most controllability also show the greatest developmental increase in control, while regions with lower controllability decrease further with age (Fig. 3a–b). We refer to these strong controllers that increase in controllability with age as ‘super-controllers’, whose putative role in the network lies in the differentiation of brain structure necessary to support the wider variety of dynamics that accompanies normative maturation.

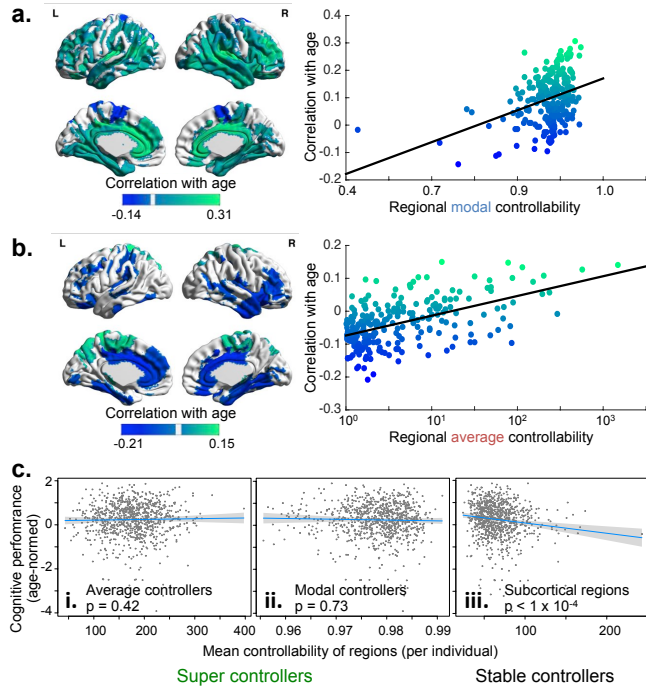


Figure 3: Regional specialization with age and its impact on cognition. (a) (Left) Regions of significantly increasing modal controllability with age (green) and significantly decreasing modal controllability with age (dark blue). (Right) The green regions tend to be stronger modal controllers (‘super-controllers’), as seen by the positive slope between the age correlation and regional modal controllability values. (b) (Left) Regions of significantly increasing average controllability with age (green) and significantly decreasing average controllability with age (dark blue). (Right) The green regions tend to be stronger average controllers (‘super-controllers’), as seen by the positive slope between the age correlation and regional average controllability values. (c.i) Super average controllers (green regions that significantly increase in controllability with age and tend to have higher average controllability) show little relation with cognitive performance (age-normed). The blue line denotes the best linear fit and the gray envelope denotes the 95% confidence interval. (c.ii) Super modal controllers also show little relation with cognitive performance. (c.iii) The regions that are most stable in controllability over development – subcortical regions – show a significant negative correlation between their average controllability and cognitive performance, suggesting that broad development in cortical regions instead, accounts for nontrivial variance in individual differences in cognition. The fits in panels (c) all control for age, brain volume, head motion, sex, and handedness.

One could argue that the regions that emerge as super-controllers over the course of development may be necessary for the high levels of cognitive function observed in adulthood. Alternatively, one could argue that these supercontrollers are unstable points in the network undergoing massive re-organization with age, and therefore that optimal predictors of individual differences in cog-

nitive function (above and beyond that expected by age) will instead be found in the regions that remain stable in their controllability over development. To test this pair of conflicting hypotheses, we examine the relationship between cognitive performance on a battery of tasks and individual differences in controllability, separately averaged over (i) super average controllers (Fig. 3c.i), (ii) super modal controllers (Fig. 3c.ii), and (iii) stable controllers (Fig. 3c.iii). While controlling for the effects of age, we observe that individuals with higher cognitive performance also display weaker stable controllers, largely located in subcortical areas (Spearman correlation coefficient between cognitive performance and mean average controllability of stable controllers $\rho = -0.14$, $df = 881$, $p < 1 \times 10^{-4}$). These results suggest that the relative strength of controllers in subcortical *versus* cortical regions is critical for understanding individual differences in overall cognitive function, i.e. a shift in control away from cortical regions may be detrimental to higher-order cognition.

Brain networks: optimized for diverse dynamics

While the fitted curves in Figs. 1d & 2b are quite remarkable, this observation does not constitute a mechanistic theory. However, they do suggest one: brain networks develop *explicitly* to maximize controllability while limiting synchronizability. To test this hypothesis, we use an evolutionary algorithm to chart a course for network evolution in the 3-dimensional space of these features (average controllability, modal controllability, and synchronizability). We employ an optimization method developed in economics and game theory, Pareto optimization, which has recently been adapted to explore brain network topologies (morphospace) [19]. Beginning with a brain network obtained from the original data, an existing edge in the network is randomly chosen for rewiring, to take the place of an edge that did not previously exist. The controllability and synchronizability metrics are calculated for that new network and if the new network is found to advance the Pareto front (see Fig. 4a), the rewiring is retained; if not the rewiring is dismissed. This process is repeated to chart a course by which networks increase controllability and decrease synchronizability, while maintaining the same edge weight distribution and mean degree. To provide contrast in the opposite direction, we evolve the subject’s network both forward in developmental time (increasing control and decreasing synchronizability), and backward in developmental time (decreasing control and increasing synchronizability).

Critically, we observe that the evolutionary trajectory that optimizes controllability and minimizes synchronizability is a constrained path that tracks the human brain data points well. These results support the hypothesis

that a mechanism of human brain development is the re-configuration of white matter connectivity to increase the human’s ability to flexibly move between diverse brain states [20, 21]. In addition to this fundamental and more general insight, we also make several specific observations. First, we observe that it is much easier to decrement the high controllability values than to increase them (Fig. 4b), as measured by the distance traversed by the evolving networks along the Pareto front (see Supplement). Similarly, it is much easier to increase synchronizability than it is to decrease it (Figs. 4c, d). These results suggest that brain networks are comparatively well-optimized for high controllability and low synchronizability – highlighting the diversity of temporal patterns and dynamics that the brain supports. Second, we observe that the final evolved values for controllability are more like the brain’s actual values than the final evolved values for synchronizability, which are in fact much lower than that observed in the brain (see Supplement). These results suggest that brain networks have near-optimal controllability, but do not fully limit synchronizability, likely because some finite amount of synchronizability is important for cognitive function.

A comparison with related network metrics such as maximum and minimum weighted degree (while preserving mean weighted degree), demonstrates the specificity of controllability metrics (see Supplement). As controllability metrics describe the propagation of dynamics in the network, they dramatically constrain evolutionary trajectories much more than simply increasing the maximum or minimum weighted node degrees. We also find that optimization using other relevant network metrics such as global efficiency and network modularity displays far less structure as compared to optimizing for controllability and synchronizability (see Supplement).

Steeper trajectories in children *versus* adults

In the previous section, we provided important evidence to support a mechanistic theory that implicates network reconfiguration towards optimal controllability as a fundamental driver of neurodevelopment. Next, we turn from the global assessment to the individual, and study the charted evolutionary trajectories of each subject to ask whether that trajectory harbors important information regarding the subject’s age and predictions regarding the subject’s abilities. We begin by studying the capacity for a brain network to adapt by estimating the tangent of the evolutionary trajectory. For each trajectory, we first fit the exponential form $y = a + b \exp(cx)$ to the average and modal controllability, and estimate the tangent of the curve at the position of the actual brain network (Fig. 5a). We observe that children from 8 to 12 years ($n=170$) display larger tangents, and therefore steeper evolutionary curves, than adults from 18 to 22

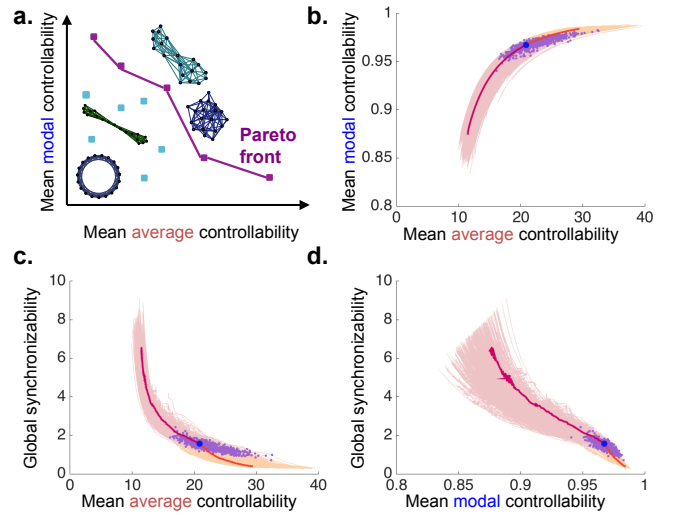


Figure 4: Brain networks are optimized for diverse

dynamics. **a.** Pareto optimization explores a family of networks with different topologies and hence varying mean controllability and synchronizability. Pareto optimal networks (dark blue) occur when these properties are most efficiently distributed, i.e., it is impossible to increase one property without decreasing another property. **b, c, d.** Beginning from an empirically measured brain network (purple dots), we swap edges to modify the topology and test if the modified network advances the Pareto front. This procedure charts a course of network evolution characterized by increasingly optimal features: here we increase mean average controllability and mean modal controllability, and decrease global synchronizability, in 1500 edge swaps (yellow curves). For comparison, we also evolved the network in the opposite direction (to decrease controllability and increase synchronizability, pink curves). The trajectory for one subject (blue dot) is highlighted (orange and red). See Methods for evidence of convergence of controllability metrics in the forward direction after 1500 edge swaps.

years ($n=190$) (Fig. 5b; non-parametric permutation test $p < 0.001$). These results suggest that children’s brain networks have a greater capacity for network evolution than adult brain networks. Interestingly, this group difference in steepness of the evolutionary curve is driven more by the change in modal controllability as a function of rewiring step (group-difference in tangent: non-parametric permutation test $p < 0.001$) than by the change in average controllability as a function of rewiring step ($p = 0.47$). These results suggest that children have a greater potential to increase their ability to make distant or difficult changes in mental state more than adults, whereas the potential to increase their nearby mental switches remains constant over development.

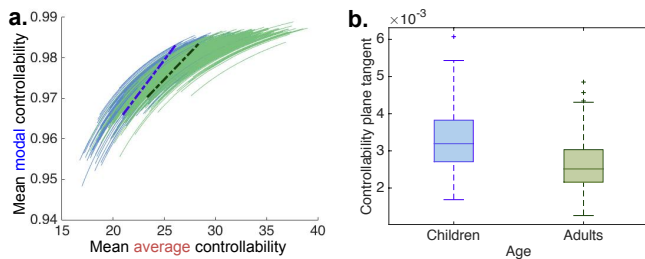


Figure 5: Steeper trajectories in children *versus* adults. **a.** We compare two cohorts of different ages, 170 children from ages 8 to 12 years (blue) and 190 adults from ages 18 to 22 years (green). Based on their forward Pareto-optimization trajectories, we fit exponential curves $y = a + b \exp(cx)$ for each subject, where x is the mean average controllability and y is the mean modal controllability, to obtain the curve tangent at the position of the brain network. The mean tangents of both groups are shown as dotted lines: the children’s in blue and the adult’s in green. **b.** The distribution of tangents for both groups shows that children have a 27% steeper slope in their optimization curves as compared to the adults; non-parametric permutation test $p < 0.001$. This difference arises from the evolutionary curve in modal controllability, suggesting that children have a greater potential for increasing their ability to make distant or difficult changes in mental state than adults (see main text).

DISCUSSION

We address the fundamental question of how the architecture of the brain supports the emergence of cognitive abilities in humans — drawing on the computational tools and conceptual frameworks of theoretical physics and engineering to study two complementary predictors of brain dynamics built from the organization of the brain’s white matter or *connectome*. Intuitively, controllability [6, 8, 22] and synchronizability [17] separately predict the brain’s ability to transition to nearby *versus* distant states, or to maintain a single state characterized by a stable temporal dynamic. While mathematically, there are no known correspondences between these two notions, we uncover evidence that the brain optimizes the former (controllability, to both near and distant states) at the expense of the latter (synchronizability). Perhaps even more notable, this optimization occurs during development in youth, and individual differences in control architecture of white matter are correlated with individual differences in cognitive performance. We use forward-modeling computational approaches [19] to identify constrained evolutionary trajectories, providing the first evidence supporting the notion that network control is a key mechanism in development [23].

Implications for Cognitive Neuroscience The results reported here provide a foundation for linking specific regional controllers to neurophysiological processes that occur over short and long distances. For example, high

modal controllers — predominantly found in executive areas — are predicted to control dynamics that extend over large distances across the brain. These inferences are consistent with and provide novel structurally-based neural mechanisms for the observed empirical function of cognitive control areas [24–26]. Specifically, cognitive control areas are thought to drive or constrain neurophysiological dynamics over distributed neural circuits using transient modulations, consistent with the role of modal controllers [23]. Conversely, high average controllers — predominantly found along the medial wall — are predicted to control dynamics that extend over shorter distances, potentially explaining the competitive relationships observed between cognitive control areas and medial portions of the default mode system [27, 28]. More generally, the role of structural connectivity underpinning these large-scale coordinated processes offers a novel dimension to computational models of cognitive control [29]. It will be important to understand how these structural drivers constrain high-frequency activity in both health and in disorders accompanied by executive deficits [30].

The theoretical links between network control and executive function are particularly intriguing in light of our observations that brains predicted to switch easily to nearby mental states are also predicted to switch easily to distant mental states. This positive relationship was unexpected; one might intuitively assume that a brain with high performance on one type of control strategy would display low performance on another. Indeed, in many computational studies of brain network architecture the common finding is that a network optimized for one type of structure (such as local clustering) will not display another type of structure (such as modular organization) [31]. Our results suggest that individual differences in network control are correlated. This may in part explain the fact that different types of cognitive abilities tend to be highly correlated: individuals who are good at one type of cognitive task tend to be good at other cognitive tasks [32].

Implications for Developmental Neuroscience. Our approach reveals the emergence of regional super-controllers as youth mature. These findings suggest a fundamental change in graph architecture that enables specialization of regional function. Indeed, structural changes in white matter microstructure within specific brain areas have previously been linked to functional specialization, largely in terms of the computations that are being performed [33]. The super-controllers we identify here broaden these intuitions to suggest more fundamentally that large-scale changes in network architecture can support the emergence of regions specialized for different types of control strategies and different length-scales of coordination. Critically, super average controllers are located in a broad swath of frontal-parietal cortex, which is well-known to support the emergence of executive functions and the acquisition of new behaviors [34]. Super

modal controllers are located in prefrontal areas that play a critical role in the emergence of cognitive control [35]. Notably, individual differences in cognitive ability – above and beyond that explained by age – are driven by relatively stable controllers in subcortical regions. These results suggest that the relative strength of controllers in subcortical *versus* cortical regions is critical for understanding individual differences in overall cognitive function, a notion that is supported by the functional segregation of these areas in the healthy adult [36]. Lastly, we note that the patterns in white matter architecture in children have a greater potential to increasingly support distant (difficult) brain state transitions, whereas the potential to support nearby (easy) brain state transitions remains constant over development.

Future Directions. Our observation that brain controllability increases during neurodevelopment suggests the existence of an optimization process that maximizes the human brain’s ability to transition among mental states while minimizing our vulnerability to being fixed in a single state. If this suggestion is in fact true, then what specific neurophysiological dynamics does this increased controllability enhance? Separately, what behavioral phenotypes would these optimizations support? Answers to these and related questions will require new directions of empirical research seeking to bridge the neurophysiological drivers of skill acquisition [37] with the control architectures that support them [10, 23]. Such studies might shed light on the question of whether structural changes enable the learning of new behaviors, or whether learning itself alters white matter architecture such that the control energy required for a task decreases as a youth matures. These questions would benefit from longitudinal empirical studies and provide a step towards characterization of healthy neurodevelopment.

Lastly, our mechanistic modeling efforts sought to investigate the rearrangement of network topology through edge swaps in the human brain network. Interestingly, this approach mimics an aspect of neural plasticity and reorganization that may naturally occur through adolescent development [38, 39]. Future work could expand on this model to take into account spatial constraints on brain network architecture, and implement addition and deletion of edges tracking the known trajectories of growth or pruning processes. While our findings support the notion that optimization of controllability is a mechanism in development, more detailed biophysical investigation is needed for a complete characterization.

-
- [1] R. E. Roberts, E. J. Anderson, and M. Husain, *Neuroscientist* **19**, 8 (2013).
 - [2] O. Sporns, G. Tononi, and R. Kotter, *PLoS Comput Biol* **1**, e42 (2005).
 - [3] H. Johansen-Berg, *Curr Opin Neurol* **23**, 351 (2010).

- [4] H. Huang, N. Shu, V. Mishra, T. Jeon, L. Chalak, Z. J. Wang, N. Rollins, G. Gong, H. Cheng, Y. Peng, Q. Dong, , and Y. He, *Cereb Cortex* **25**, 1389 (2015).
- [5] G. L. Baum, R. Ciric, D. R. Roalf, R. F. Betzel, T. M. Moore, R. T. Shinohara, A. E. Kahn, M. Quarmley, P. A. Cook, M. A. Elliot, K. Ruparel, R. E. Gur, R. C. Gur, D. S. Bassett, and T. D. Satterthwaite, *arXiv* **1608**, 03619 (2016).
- [6] K. J. Reinschke, *Multivariable Control: A Graph-Theoretic Approach* (Springer, 1988).
- [7] R. E. Kalman, Y. C. Ho, and K. S. Narendra, *Contributions to Differential Equations* **1**, 189 (1963).
- [8] T. Kailath, *Linear Systems* (Prentice-Hall, 1980).
- [9] L. M. Pecora and T. L. Carroll, *Phys. Rev. Lett.* **80**, 2109 (1998).
- [10] F. Pasqualetti, S. Zampieri, and F. Bullo, *Control of Network Systems*, *IEEE Transactions on* **1**, 40 (2014).
- [11] M. Senden, G. Deco, M. A. de Reus, R. Goebel, and M. P. van den Heuvel, *Neuroimage* **96**, 174 (2014).
- [12] N. Kopell, G. B. Ermentrout, M. A. Whittington, and R. D. Traub, *Proc Natl Acad Sci U S A* **97**, 1867 (2000).
- [13] P. Fries, *Trends Cogn Sci* **9**, 474 (2005).
- [14] P. Fries, *Neuron* **88**, 220 (2015).
- [15] A. N. Khambhati, K. A. Davis, B. S. Oommen, S. H. Chen, T. H. Lucas, B. Litt, and D. S. Bassett, *PLoS Comput Biol* **11**, e1004608 (2015).
- [16] A. N. Khambhati, K. A. Davis, T. H. Lucas, B. Litt, and D. S. Bassett, *Neuron* **In Press** (2016).
- [17] M. Barahona and L. M. Pecora, *Phys Rev Lett* **89**, 054101 (2002).
- [18] T. Nishikawa and A. E. Motter, *Proceedings of the National Academy of Sciences* **107**, 10342 (2010).
- [19] A. Avena-Koenigsberger, J. Goni, R. F. Betzel, M. P. van den Heuvel, A. Griffa, P. Hagmann, J. P. Thiran, and O. Sporns, *Philos Trans R Soc Lond B Biol Sci* **369**, 20130530 (2014).
- [20] J. D. Medaglia, T. D. Satterthwaite, T. M. Moore, K. Ruparel, R. C. Gur, R. E. Gur, and D. S. Bassett, *arXiv* **1510**, 08780 (2015).
- [21] L. Chai, A. N. Khambhati, R. C. Gur, R. E. Gur, T. D. Satterthwaite, and D. S. Bassett, *Network Neuroscience* **Submitted** (2016).
- [22] R. E. Kalman, Y. C. Ho, and S. K. Narendra, *Contributions to Differential Equations* **1**, 189 (1963).
- [23] S. Gu, F. Pasqualetti, M. Cieslak, Q. K. Telesford, B. Y. Alfred, A. E. Kahn, J. D. Medaglia, J. M. Vettel, M. B. Miller, S. T. Grafton, *et al.*, *Nature communications* **6** (2015).
- [24] U. Braun, A. Schafer, H. Walter, S. Erk, N. Romanczuk-Seiferth, L. Haddad, J. I. Schweiger, O. Grimm, A. Heinz, H. Tost, A. Meyer-Lindenberg, and D. S. Bassett, *Proc Natl Acad Sci U S A* **112**, 11678 (2015).
- [25] G. Wallis, M. Stokes, H. Cousijn, M. Woolrich, and A. C. Nobre, *J Cogn Neurosci* **27**, 2019 (2015).
- [26] M. D. Sacchet, R. A. LaPlante, Q. Wan, D. L. Pritchett, A. K. Lee, M. Hamalainen, C. I. Moore, C. E. Kerr, and S. R. Jones, *J Neurosci* **35**, 2074 (2015).
- [27] A. Fornito, A. Zalesky, C. Pantelis, and E. T. Bullmore, *Neuroimage* **62**, 2296 (2012).
- [28] T. D. Satterthwaite, D. H. Wolf, G. Erus, K. Ruparel, M. A. Elliott, E. D. Gennatas, R. Hopson, C. Jackson, K. Prabhakaran, W. B. Bilker, M. E. Calkins, J. Loughead, A. Smith, D. R. Roalf, H. Hakonarson, R. Verma, C. Davatzikos, R. C. Gur, and R. E. Gur, *The Journal*

- of Neuroscience **33**, 16249 (2013).
- [29] M. M. Botvinick and J. D. Cohen, Cogn Sci **38**, 1249 (2014).
- [30] B. R. Pittman-Polletta, B. Kocsis, S. Vijayan, M. A. Whittington, and N. J. Kopell, Biol Psychiatry **77**, 1020 (2015).
- [31] F. Klimm, D. S. Bassett, J. M. Carlson, and P. J. Mucha, PLoS Comput Biol **10**, e1003491 (2014).
- [32] A. Miyake, N. P. Friedman, M. J. Emerson, A. H. Witzki, A. Howerter, and T. D. Wager, Cognitive Psychology **41**, 49 (2000).
- [33] K. Jarbo and T. D. Verstynen, J Neurosci **35**, 3865 (2015).
- [34] E. G. Chrysikou, J. M. Novick, J. C. Trueswell, and S. L. Thompson-Schill, Top Cogn Sci **3**, 253 (2011).
- [35] K. L. Seghete, M. M. Herting, and B. J. Nagel, Brain Res **1527**, 15 (2013).
- [36] L. Cerliani, M. Mennes, R. M. Thomas, A. Di Martino, M. Thioux, and C. Keysers, JAMA Psychiatry **72**, 767 (2015).
- [37] E. Dayan and L. G. Cohen, Neuron **72**, 443 (2011).
- [38] A. Mitra, S. S. Mitra, and R. W. Tsien, Nat Neurosci **15**, 250 (2012).
- [39] A.-K. Brem, P. J. Fried, J. C. Horvath, E. M. Robertson, and A. Pascual-Leone, NeuroImage **85**, Part 3, 1058 (2014), neuro-enhancement.
- [40] T. D. Satterthwaite, M. A. Elliott, K. Ruparel, J. Loughead, K. Prabhakaran, M. E. Calkins, R. Hopson, C. Jackson, J. Keefe, M. Riley, F. D. Mentch, P. Sleiman, R. Verma, C. Davatzikos, H. Hakonarson, R. C. Gur, and R. E. Gur, NeuroImage **86**, 544 (2014).
- [41] T. D. Satterthwaite, J. J. Connolly, K. Ruparel, M. E. Calkins, C. Jackson, M. A. Elliott, D. R. Roalf, R. Hopson, K. Prabhakaran, M. Behr, H. Qiu, F. D. Mentch, R. Chiavacci, P. M. Sleiman, R. C. Gur, H. Hakonarson, and R. E. Gur, NeuroImage **124**, Part B, 1115 (2016).
- [42] D. R. Roalf, M. Quarmley, M. A. Elliott, T. D. Satterthwaite, S. N. Vandekar, K. Ruparel, E. D. Gennatas, M. E. Calkins, T. M. Moore, R. Hopson, K. Prabhakaran, C. T. Jackson, R. Verma, H. Hakonarson, R. C. Gur, and R. E. Gur, NeuroImage **125**, 903 (2016).
- [43] M. E. Calkins, K. R. Merikangas, T. M. Moore, M. Burstein, M. A. Behr, T. D. Satterthwaite, K. Ruparel, D. H. Wolf, D. R. Roalf, F. D. Mentch, H. Qiu, R. Chiavacci, J. J. Connolly, P. M. Sleiman, R. C. Gur, H. Hakonarson, and R. E. Gur, Journal of Child Psychology and Psychiatry **56**, 1356 (2015).
- [44] S. N. Vandekar, R. T. Shinohara, A. Raznahan, D. R. Roalf, M. Ross, N. DeLeo, K. Ruparel, R. Verma, D. H. Wolf, R. C. Gur, R. E. Gur, and T. D. Satterthwaite, The Journal of Neuroscience **35**, 599 (2015).
- [45] T. M. Moore, S. P. Reise, R. E. Gur, H. Hakonarson, and R. C. Gur, Neuropsychology **29**, 235 (2015).
- [46] A. Daducci, S. Gerhard, A. Griffa, A. Lemkaddem, L. Cammoun, X. Gigandet, R. Meuli, P. Hagmann, and J.-P. Thiran, PLoS ONE **7**, 1 (2012).
- [47] A. M. Dale, B. Fischl, and M. I. Sereno, NeuroImage **9**, 179 (1999).
- [48] D. S. Bassett, J. A. Brown, V. Deshpande, J. M. Carlson, and S. T. Grafton, Neuroimage **54**, 1262 (2011).
- [49] C. O. Becker, S. Pequito, G. J. Pappas, M. B. Miller, S. T. Grafton, D. S. Bassett, and V. M. Preciado, ArXiv e-prints (2015), arXiv:1512.02602 [q-bio.NC].
- [50] M. M. Bohlken, R. M. Brouwer, R. W. Mandl, and et al, JAMA Psychiatry **73**, 11 (2016).
- [51] S. T. Baker, D. I. Lubman, M. Ycel, N. B. Allen, S. Whittle, B. D. Fulcher, A. Zalesky, and A. Fornito, **35**, 9078 (2015).
- [52] S. Gu, T. D. Satterthwaite, J. D. Medaglia, M. Yang, R. E. Gur, R. C. Gur, and D. S. Bassett, Proc Natl Acad Sci U S A **112**, 13681 (2015).
- [53] C. J. Honey, O. Sporns, L. Cammoun, X. Gigandet, J. P. Thiran, R. Meuli, and P. Hagmann, Proc Natl Acad Sci U S A **106**, 2035 (2009).
- [54] R. Fernández Galán, PLoS One **3**, e2148 (2008).
- [55] R. E. Kalman, Y. C. Ho, and S. K. Narendra, Contrib. Differ. Equat. **1**, 189213 (1963).
- [56] B. Marx, D. Koenig, and D. Georges, in *American Control Conference* (Boston, MA, USA, 2004) pp. 2729–2734.
- [57] H. R. Shaker and M. Tahavori, Journal of Vibration and Control (2012).
- [58] T. Kailath, *Linear systems*, Vol. 1 (Prentice-Hall Englewood Cliffs, NJ, 1980).
- [59] A. M. A. Hamdan and A. H. Nayfeh, AIAA Journal of Guidance, Control, and Dynamics **12**, 421 (1989).
- [60] F. Pasqualetti, S. Zampieri, and F. Bullo, IEEE Transactions on Control of Network Systems **1**, 40 (2014).
- [61] L. Huang, Q. Chen, Y.-C. Lai, and L. M. Pecora, Phys. Rev. E **80**, 036204 (2009).
- [62] M. Chen and M. W. Deem, Physical Biology **12**, 016009 (2015).
- [63] P. Hagmann, O. Sporns, N. Madan, L. Cammoun, R. Pienaar, V. J. Wedeen, R. Meuli, J.-P. Thiran, and P. E. Grant, Proceedings of the National Academy of Sciences **107**, 19067 (2010).
- [64] P. J. Mucha, T. Richardson, K. Macon, M. A. Porter, and J.-P. Onnela, Science **328**, 876 (2010).
- [65] P. Hagmann, L. Cammoun, X. Gigandet, R. Meuli, C. J. Honey, V. J. Wedeen, and O. Sporns, PLoS Biol **6**, 1 (2008).
- [66] T. E. J. Behrens, H. Johansen-Berg, M. W. Woolrich, S. M. Smith, C. A. M. Wheeler-Kingshott, P. A. Boulby, G. J. Barker, E. L. Sillery, K. Sheehan, O. Ciccarelli, A. J. Thompson, J. M. Brady, and P. M. Matthews, Nat Neurosci **6**, 750 (2003).
- [67] L. Li, J. K. Rilling, T. M. Preuss, M. F. Glasser, and X. Hu, Human Brain Mapping **33**, 1894 (2012).
- [68] T. Behrens, H. J. Berg, S. Jbabdi, M. Rushworth, and M. Woolrich, NeuroImage **34**, 144 (2007).
- [69] J. M. Duarte-Carvajalino, N. Jahanshad, C. Lenglet, K. L. McMahon, G. I. de Zubicaray, N. G. Martin, M. J. Wright, P. M. Thompson, and G. Sapiro, Neuroimage **59**, 3784 (2012).

METHODS

Subject Sample

Diffusion tensor imaging (DTI) data were acquired from the Philadelphia Neurodevelopmental Cohort (PNC), a large community-based study of brain development. All MRI scans were acquired on the same 3 T Siemens Tim Trio whole-body scanner and 32-channel head coil at the Hospital of the University of Pennsylvania. DTI scans were obtained using a twice-

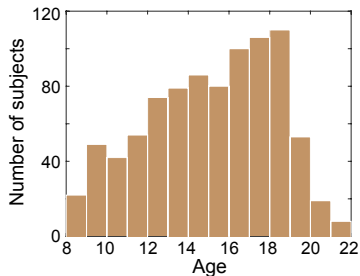


Figure 6: Histogram of subject ages. We examine 882 healthy individuals from the ages of 8 to 22.

refocused spin-echo (TRSE) single-shot EPI sequence (TR = 8100ms, TE = 82ms, FOV = 240mm²/240mm²; Matrix = RL: 128/AP:128/Slices:70, in-plane resolution (x & y) 1.875 mm²; slice thickness = 2mm, gap = 0; FlipAngle = 90°/180°/180°, volumes = 71, GRAPPA factor = 3, bandwidth = 2170 Hz/pixel, PE direction = AP). The sequence employs a four-lobed diffusion encoding gradient scheme combined with a 90-180-180 spin-echo sequence designed to minimize eddy-current artifacts. The complete sequence consisted of 64 diffusion-weighted directions with $b = 1000\text{s/mm}^2$ and 7 interspersed scans where $b = 0\text{s/mm}^2$. Scan time was approximately 11 min. The imaging volume was prescribed in axial orientation covering the entire cerebrum with the topmost slice just superior to the apex of the brain [40–43].

This study includes 882 subjects between 8–22 years old (mean age=15.06, SD=3.15, see Fig. 6; 389 males, 493 females) who had no gross radiological abnormalities that distorted brain anatomy, no history of inpatient psychiatric hospitalization, no use of psychotropic medications at the time of scanning, and no medical disorders that could impact brain function. Each of the 882 included subjects also passed both manual and automated quality-assessment protocols for DTI [42] and T1-weighted structural imaging [44], and had low in-scanner head motion (less than 2mm mean relative displacement between $b=0$ volumes). Cognitive scores were measured using tests from the Penn Computerized Neurocognitive Battery, from which a bifactor analysis revealed a summary efficiency score that we utilized as a measure of subject cognitive performance [45].

Connectome Construction

Structural connectivity was estimated using 64-direction DTI data. The diffusion tensor was estimated and deterministic whole-brain fiber tracking was implemented in DSI Studio using a modified FACT algorithm, with exactly 1,000,000 streamlines initiated per subject after removing all streamlines with length less

than 10mm [23]. A 234-region parcellation [46] was constructed from the T1 image using FreeSurfer [47]. Parcels were dilated by 4mm to extend regions into white matter [48], and registered to the first non-weighted ($b=0$) volume using an affine transform. Edge weights A_{ij} in the adjacency matrix were defined by the number of streamlines connecting each pair of nodes end-to-end [49–51]. All analyses were replicated using an alternative edge weight definition, where weights are equal to the number of streamlines connecting each node pair divided by the total volume of the node pair [51], as well as using probabilistic fiber tracking methods (see following section). The schematic for structural connectome construction is depicted in Fig. 1a.

Brain regions within the 234-region parcellation can be assigned to anatomical and cognitive systems [52]. We use this assignment to identify 14 subcortical brain regions in both the left and right hemispheres: the thalamus proper, caudate, putamen, pallidum, accumbens area, hippocampus and amygdala.

Network controllability

A networked system can be represented by the graph $\mathcal{G} = (\mathcal{V}, \mathcal{E})$, where \mathcal{V} and \mathcal{E} are the vertex and edge sets, respectively. Let a_{ij} be the weight associated with the edge $(i, j) \in \mathcal{E}$, and define the *weighted adjacency matrix* of \mathcal{G} as $A = [a_{ij}]$, where $a_{ij} = 0$ whenever $(i, j) \notin \mathcal{E}$. We associate a real value (*state*) with each node, collect the node states into a vector (*network state*), and define the map $x : \mathbb{N}_{\geq 0} \rightarrow \mathbb{R}^n$ to describe the evolution (*network dynamics*) of the network state over time.

In our case, $\mathbf{A} \in \mathbb{R}^{N \times N}$ is a symmetric and weighted adjacency matrix whose elements indicate the number of white matter streamlines connecting two different brain regions — denoted here as i and j . An underlying assumption of this approach is that the number of streamlines is proportional to the strength of structural connectivity.

Dynamical model

The equation of state that we utilize is based on extensive prior work demonstrating its utility in predicting resting state functional connectivity [53] and in providing similar brain dynamics to more complicated models [54]. Although neural activity evolves through neural circuits as a collection of *nonlinear* dynamic processes, these prior studies have demonstrated that a significant amount of variance in neural dynamics as measured by fMRI can be predicted from simplified *linear* models.

Based on this literature, we employ a simplified noise-free linear discrete-time and time-invariant network

model [23]:

$$\mathbf{x}(t+1) = \mathbf{A}\mathbf{x}(t) + \mathbf{B}_\mathcal{K}\mathbf{u}_\mathcal{K}(t), \quad (1)$$

where $\mathbf{x} : \mathbb{R}_{\geq 0} \rightarrow \mathbb{R}^N$ describes the state (i.e., a measure of the electrical charge, oxygen level, or firing rate) of brain regions over time, and $\mathbf{A} \in \mathbb{R}^{N \times N}$ is the structural connectome described in the previous section. Note that to assure Schur stability, we divide the matrix by $1 + \xi_0(A)$, where $\xi_0(A)$ is the largest singular value of \mathbf{A} .

The diagonal elements of the matrix \mathbf{A} satisfy $A_{ii} = 0$. The input matrix $\mathbf{B}_\mathcal{K}$ identifies the control points \mathcal{K} in the brain, where $\mathcal{K} = \{k_1, \dots, k_m\}$ and

$$\mathbf{B}_\mathcal{K} = [e_{k_1} \ \cdots \ e_{k_m}], \quad (2)$$

and e_i denotes the i -th canonical vector of dimension N . The input $\mathbf{u}_\mathcal{K} : \mathbb{R}_{\geq 0} \rightarrow \mathbb{R}^m$ denotes the control strategy.

We study the *controllability* of this dynamical system, which refers to the possibility of driving the state of the system to a specific target state by means of an external control input [55]. Classic results in control theory ensure that controllability of the network (1) from the set of network nodes \mathcal{K} is equivalent to the controllability Gramian $\mathbf{W}_\mathcal{K}$ being invertible, where

$$\mathbf{W}_\mathcal{K} = \sum_{\tau=0}^{\infty} \mathbf{A}^\tau \mathbf{B}_\mathcal{K} \mathbf{B}_\mathcal{K}^\top \mathbf{A}^\tau. \quad (3)$$

Consistent with [23], we utilize this framework to choose control nodes one at a time, and thus the input matrix \mathbf{B} in fact reduces to a one-dimensional vector. While the model we employ is a discrete-time system, this controllability Gramian is statistically similar to that obtained in a continuous-time system [23].

Controllability metrics

Within this controllability framework, we study two different control strategies that describe the ability to move the network into different states defined as patterns of regional activity (Fig. 1bi). Average controllability describes the ease of transition to many states nearby on an energy landscape, while modal controllability describes the ease of transition to a state distant on this landscape.

Average controllability of a network equals the average input energy from a set of control nodes and over all possible target states [56, 57]. As a known result, average input energy is proportional to $\text{Trace}(\mathbf{W}_\mathcal{K}^{-1})$, the trace of the inverse of the controllability Gramian. Instead and consistent with [23], we adopt $\text{Trace}(\mathbf{W}_\mathcal{K})$ as a measure of average controllability for two main reasons: first, $\text{Trace}(\mathbf{W}_\mathcal{K}^{-1})$ and $\text{Trace}(\mathbf{W}_\mathcal{K})$ satisfy a relation of inverse proportionality, so that the information obtained from the two metrics are correlated with one another

and, second, $\mathbf{W}_\mathcal{K}$ is typically very ill-conditioned even for coarse network resolutions, so that $\text{Trace}(\mathbf{W}_\mathcal{K}^{-1})$ cannot be accurately computed even for small brain networks. It should be noted that $\text{Trace}(\mathbf{W}_\mathcal{K})$ encodes a well-defined control metric, namely the energy of the network impulse response or, equivalently, the network H_2 norm [58].

Modal controllability refers to the ability of a node to control each evolutionary mode of a dynamical network [59], and can be used to identify states that are difficult to control from a set of control nodes. Modal controllability is computed from the eigenvector matrix $\mathbf{V} = [v_{ij}]$ of the network adjacency matrix \mathbf{A} . By extension from the PBH test [58], if the entry v_{ij} is small, then the j -th mode is poorly controllable from node i . Following [60], we define $\phi_i = \sum_j (1 - \xi_j^2(A)) v_{ij}^2$ as a scaled measure of the controllability of all N modes $\xi_0(A), \dots, \xi_{N-1}(A)$ from the brain region i . Regions with high modal controllability are able to control all the dynamic modes of the network, and hence to drive the dynamics towards hard-to-reach configurations.

Network synchronizability

Synchronizability measures the ability of a network to persist in a single synchronous state $\mathbf{s}(t)$, i.e. $\mathbf{x}_1(t) = \dots = \mathbf{x}_n(t+1) = \mathbf{s}(t)$ (see Fig. 2a in main text). The master stability function (MSF) allows analysis of the stability of this synchronous state without detailed specification of the properties of the dynamical units [9]. Within this framework, linear stability depends on the positive eigenvalues $\{\lambda_i\}, i = 1, \dots, N-1$ of the Laplacian matrix \mathbf{L} defined by $L_{ij} = \delta_{ij} \sum_k A_{ik} - A_{ij}$.

The condition for stability depends on the shape of the MSF and whether these eigenvalues fall into the region of stability. Hence we can use the normalized spread of the eigenvalues to quantify how synchronizable the network will generally be [18]. We therefore quantify network synchronizability as

$$\frac{1}{\sigma^2} = \frac{d^2(N-1)}{\sum_{i=1}^{N-1} |\lambda_i - \bar{\lambda}|^2}, \quad \text{where } \bar{\lambda} := \frac{1}{N-1} \sum_{i=1}^{N-1} \lambda_i \quad (4)$$

and $d := \frac{1}{N} \sum_i \sum_{j \neq i} A_{ij}$, the average coupling strength per node, which normalizes for the overall network strength.

We have plotted a typical example of a MSF for a network of oscillators schematically in Fig. 2a; however, specific details will depend on the dynamics on individual nodes and the connectivity between them. The shape of the MSF for various families of dynamical systems is typically convex for generic oscillator systems, including chaotic oscillators that have stable limit cycles [61].

Network statistics and curve-fitting

Pearson correlations were predominantly used except where the data distribution was markedly skewed, in which case Spearman correlations were used instead (regional modal controllability and cognitive performance). Regional controllability values were the mean controllability values over all individuals: 190 subjects aged 18 and above in Fig. 2, and all 882 subjects in Fig. 3, both in the main text. To test for the regional significance of correlation with age in Fig. 3, a false discovery rate correction for multiple comparisons was used with $q = 0.05$.

Curve fitting was done using the Curve Fitting Toolbox in MATLAB. We chose exponential fits for all data and optimization trajectories as three parameters in each case produced good fits. However, the Pareto optimization trajectories are not really exponential, i.e. taking the log of one of the variables does not make the relationship linear. Hence we simply left all plots in their original axes and used exponential fits.

Pareto-optimization parameters

The trajectories traced out by Pareto-optimization can be very constrained in the paths they delineate and especially in the forward direction of mean average controllability and mean modal controllability. We always ran 100 parallel computations each with their own random edge swaps, and in this direction of forward optimization for controllability all the curves followed the same path. Curve-fitting was done only on trajectories in this direction, for which we simply picked one trajectory out of the 100 similar ones.

Termination of the Pareto-optimization process was done after 1500 evolutionary steps, by which time the controllability metrics showed comparatively small changes from one step to the next. The mean absolute value of changes in controllability metrics for the last 500 steps were below 1% of the total change in either mean average controllability or mean modal controllability, for the average subject.

Trajectories in the synchronizability cross-sections and backward direction showed greater variability among the parallel simulations. In the backwards direction, after a smooth decrease in controllability for many steps, some curves began to turn around or display erratic jumps, see Fig. 7 for trajectories chosen at random from each subject. These backward trajectories were truncated when the gradient in the controllability plane (change of mean modal controllability over change in mean average controllability) became negative. We then retained the longest trajectory (visualized in Fig. 4 of the main text), although in most cases there was little loss of overall trajectory length.

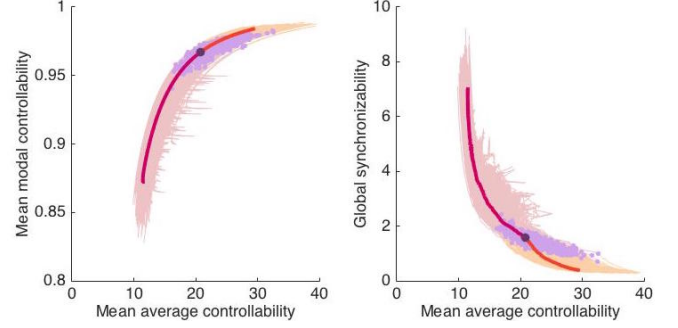


Figure 7: Trajectories without truncation. While Pareto optimization trajectories in the forward direction (yellow) display very smooth curves, trajectories in the backwards direction (pink) do not. These trajectories were truncated where the curve gradient in the controllability plane (left plot) became negative, often resulting in little loss of overall trajectory length.

OPTIMIZATION OF BRAIN NETWORKS

Here we investigate the trajectories traced out by evolving networks upon optimizing for controllability and synchronizability metrics. First, we demonstrate that brain networks are well optimized for high controllability and low synchronizability by comparing distances travelled in the forward and backward directions. Second, we compare the evolved metrics with the data to show brain networks can reach near-optimal values of controllability but seem to saturate at a finite level of synchronizability.

Brain networks are well-optimized for high controllability and low synchronizability

Our Pareto-optimization algorithm runs for 1500 edge steps in both the forward (optimizing for high average and modal controllabilities, and low synchronizability) and backward (optimizing for low average and modal controllabilities and high synchronizability) directions. An estimate of the discrete distance traveled in the forward direction is

$$d_f = \sqrt{\left(\frac{x_f}{x_0}\right)^2 + \left(\frac{y_f}{y_0}\right)^2 + \left(\frac{z_f}{z_0}\right)^2} \quad (5)$$

where x is mean average controllability, y is mean modal controllability and z is synchronizability. This is a dimensionless distance, normalized by the total distance travelled, i.e. $x_0 = x_f - x_b$, where x_f and x_b are changes in the forward and backward directions, respectively. Similarly, we can write a similar expression for the dimensionless distance in the backward direction by replacing $f \rightarrow b$ in the above expression. The ratio of distance traveled forward to backward is then d_f/d_b .

Examining first the average controllability *versus*

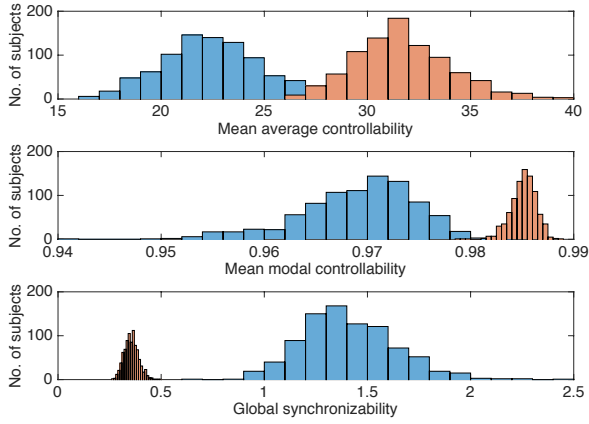


Figure 8: Brain networks show near-optimal control but finite synchronizability. The original brain networks (blue) and final evolved networks (orange) show overlap between their controllability values (first and second plots), however there is no overlap between the synchronizability values of these two groups (third plot) — suggesting that brain networks display near optimal control but retain a finite level of synchronizability.

modal controllability plane (Fig. 4b in main text and setting $z = 0$ in the expression above), we find that this ratio is 0.52, so it is almost twice as easy to decrement the controllability values than to increase them. Including synchronizability as well in the full three-dimensional space (Figs. 4c–d in main text), we find that this ratio is 0.46, indicating that it is also markedly easier to increase synchronizability than to decrease it. These results indicate that within the space of networks with the same edge distribution, brain networks have topologies that are well optimized for high controllability and low synchronizability.

Brain networks are near optimal for controllability

Final evolved values for controllability are more like actual values shown by brain networks than are the final evolved values for synchronizability, see Fig. 8. This suggests that brain networks have near-optimal controllability, but do not fully limit synchronizability, perhaps because some finite amount of synchronization is needed for dynamical coordination and cognition.

PARETO OPTIMIZATION WITH OTHER METRICS

In this section, we examine if the developmental arcs seen with controllability and synchronizability could be produced by calculating similar or other suitable network metrics on brain networks. We examine these two possibilities separately: firstly, with metrics that contain

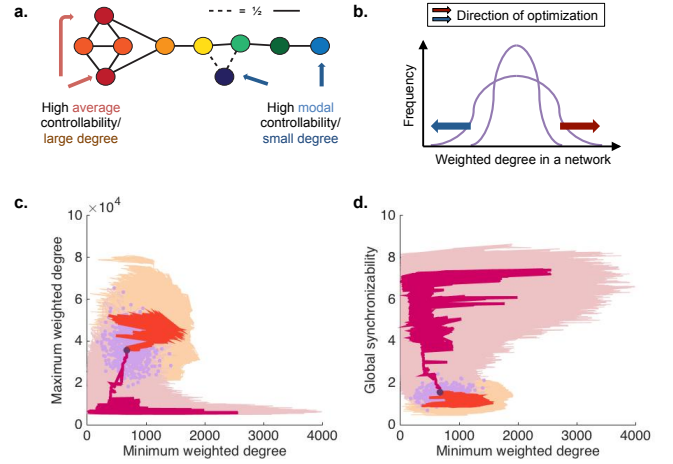


Figure 9: Specificity of controllability *versus* degree.

a. As average (modal) controllability of each node is closely tied to high (low) weighted degree of that node [23], we repeat our optimization for maximum and minimum weighted degree in the network. **b.** While the edge weight distribution of the network remains the same, edge swaps can alter the total degree of each node to increase the minimum (blue arrow) or maximum (red arrow) degree of the nodes. **c, d.** The maximum and minimum weighted degree of each subject’s brain network are plotted as purple dots (**c.**) and similarly for minimum weighted degree and synchronizability (**d.**) — we see little structure or discernible relationship between individuals. We also plot representative optimization trajectories for each subject in the forward direction (yellow) in the cross section of increasing maximum weighted degree and decreasing minimum weighted degree (**c.**) and decreasing minimum weighted degree and synchronizability (**d.**); as well as trajectories in the opposite direction (pink). The trajectory for a single representative individual is highlighted, for both forward (red) and backward (dark red) directions. We observe that this example trajectory takes a meandering path through the plane, displaying little structure.

strong overlaps with controllability (maximum and minimum weighted degree, respectively), and secondly with network metrics associated with development (global efficiency and modularity, respectively). In comparison to the complete set of available models, we demonstrate that brain networks are structured in a manner best described as highly optimized for the control of diverse neural dynamics.

Weighted degree distribution

The weighted degree of each node has a strong overlap with the controllability of that node, see Fig. 9a. Weighted degree is the sum of all the edges connected to that node; given the adjacency matrix A_{ij} it is $\sum_j A_{ij}$ for node i . The average controllability of a node has a strong positive correlation with weighted degree and the modal

controllability of a node has a strong negative correlation with weighted degree [23].

Hence, a matrix that simultaneously increases mean average controllability and mean modal controllability can be partially understood as a matrix that increases its largest and smallest weighted degree – the degree distribution has been stretched out (Fig. 9b). While our edge swapping procedure does not alter the edge weight distribution or mean weighted degree of the network, the total degree of each node can be altered to increase the minimum or maximum weighted degree respectively. We repeat our simulations now optimizing for increase of maximum weighted degree, and decrease of minimum weighted degree and global synchronizability. If controllability is merely a proxy for weighted degree, then this should give similar results to the simulations reported in the main text that optimize for increased controllability and decreasing synchronizability.

First, we observe that plotting the raw data according to maximum and minimum weighted degree (purple dots in Fig. 9c) reveals very little structure, unlike the clean developmental arc seen in Fig. 1d in the main text. This is also true for the plot of minimum weighted degree and global synchronizability (purple dots in Fig. 9d), where this is little discernible relationship, unlike the clean developmental arc shown in Fig. 2b in the main text. Second, instead of the constrained curves we see in the forward trajectories of Fig. 3 in the main text that mimic the developmental arc, now the paths simply move in a noisy manner across the plane (Fig. 9c, d: forward trajectories in yellow and backward trajectories in pink). In the highlighted trajectory for a single individual (orange and red) we see that this curve zigzags across the plane. Moreover, trajectories from separate simulations do not overlap with one another as do trajectories from separate simulations that optimize for controllability metrics.

Together, these results demonstrate that controllability metrics are far more constrained than weighted degree, or rather, high weighted degree appears to be necessary but not sufficient for average controllability, and similarly for low weighted degree and modal controllability. The derivation of controllability metrics comes from a specific dynamical model that utilizes network connectivity for the propagation of dynamics, and is far more constraining than simply having many large driver nodes or many poorly connected nodes.

Global efficiency and modularity

It is likely that brain networks also change in other ways across development, for instance they may optimize for global efficiency or change in modularity with age [62, 63]. Here we repeat the Pareto optimization in two dimensions to optimize for global efficiency and modularity, to examine if notable trends emerge that describe

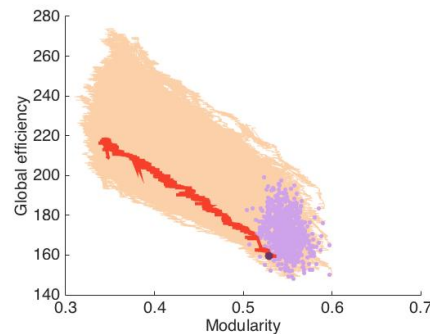


Figure 10: Optimization for efficiency and modularity. We also examine Pareto-optimization in the forward direction for the network metrics of global efficiency and modularity, that can be associated with development. Purple dots are these metrics calculated on individual brain networks, while the yellow curves indicate forward trajectories upon optimization for these two quantities; little meaningful structure is observed. The purple dot and red trajectory indicate the result for a single individual for illustration purposes.

development. To calculate global efficiency, the function *efficiency_wel* from the Brain Connectivity Toolbox was used, while a generalized Louvain-like locally greedy community detection method was used to optimize modularity, by comparison with a standard Newman-Girvan null model [64].

We optimize for these two quantities in a two-dimensional space for 1500 iterations in the forward direction, where we find that separate trajectories for the same subject have a strong overlap. Again, we see a lack of clear structure for individual variation over these quantities, as well as in the space explored in optimization, see Fig. 10. These simulations indicate that controllability and synchronizability metrics show markedly more structure for individual variation and development-related effects.

REPLICATION OF RESULTS

Adult subsample

In order to separate our findings on individual variability displayed in controllability and synchronizability and verify that they hold independent of developmental effects, here we examine only the 190 subjects aged 18 and older. By repeating the analyses just on this subject group, we can verify if they already replicate the relationships shown in controllability and synchronizability metrics.

Adults whose brains display high average controllability also tend to display high modal controllability: Pearson’s correlation coefficient $r = 0.85$, $df = 189$, $p < 1 \times 10^{-5}$. Further, the brain networks that are more

synchronizable tend to display lower average controllability ($r = -0.84$, $df = 189$, $p < 1 \times 10^{-5}$;) as well as lower modal controllability ($r = -0.78$, $df = 189$, $p < 1 \times 10^{-5}$). Hence, this smaller adult sample demonstrates well these relationships between controllability and synchronizability, independent of age-related effects. In subsequent sections below, we continue to first examine this smaller adult sample as well as developmental trends across the entire youth sample.

Controlling for network strength

As networks with higher strength (weighted degree, or sum of all edge weights) tend to have higher average controllability values, here we verify that network strength is not a confound in our results. We do this by first dividing each network by its average strength, to ensure that each matrix has the same average strength of 1 — then repeat our analysis. We find that the 190 adults show an even stronger correlation between mean average controllability and mean modal controllability: Pearson’s correlation coefficient $r = 0.89$, $df = 189$, $p < 1 \times 10^{-5}$. These controllability metrics continue to display strong negative correlations with synchronizability: $r = -0.85$, $df = 189$, $p < 1 \times 10^{-5}$ for mean average controllability and $r = -0.78$, $df = 189$, $p < 1 \times 10^{-5}$ for mean modal controllability respectively.

In the larger youth sample from ages 8 to 22, the relationships between controllability metrics and age also persist. Mean average controllability remains positively correlated with age ($r = 0.32$, $df = 881$, $p < 1 \times 10^{-5}$) and mean modal controllability does as well ($r = 0.22$, $df = 881$, $p < 1 \times 10^{-5}$). As synchronizability is calculated independent of the matrix normalization, that result remains unchanged. All these results control for sex, brain volume, handedness and head motion. The emergence of ‘super-controllers’ – regions of higher average and modal controllability that increase more with age, is also still present. Regions that display increasing average controllability with age are positively correlated with their average controllability values: $r = 0.50$, $df = 233$, $p < 1 \times 10^{-5}$, just as regions that display increasing modal controllability with age are also positively correlated with their modal controllability values: $r = 0.37$, $df = 233$, $p < 1 \times 10^{-5}$. Lastly, the stable controllers in the subcortical region still show a negative correlation between the mean average controllability in those regions, and the subject’s IQ (Spearman correlation coefficient $\rho = -0.14$, $df = 881$, $p < 1 \times 10^{-5}$, controlling for age, sex, brain volume, handedness and head motion). Together, these results show that accounting for network strength does not change (or can improve) the results we obtain in the main text. While average network strength does contribute to network controllability measures, it cannot account for our findings, which

depend on the particular network topology even given the same average network strength.

Subjects with lowest in-scanner head motion

Our work employs stringent restrictions to rule out head motion during the scanning procedure as a potential confounding factor, by ensuring that data have passed rigorous visual and automatic quality assurance to detect head motion [42]. We excluded subjects with in-scanner head motion of above 2mm (see Methods) and controlled for motion in all analyses using the 882 subject sample.

As a last check, we verify that the significant results we observe across the entire sample are replicable on the 200 subjects with the lowest head motion. While all 882 subjects have an average head motion of 0.45mm mean relative displacement, here we retain the 200 subjects with the lowest relative head motion (below 0.22mm) to replicate our findings. We find that these subjects with lowest in-scanner head motion still display a positive correlation between whole-brain average and modal controllabilities (Pearson’s correlation coefficient $r = 0.86$, $df = 199$, $p < 1 \times 10^{-5}$), while synchronizability remains negatively correlated with both mean average and modal controllabilities ($r = -0.84$, $df = 199$, $p < 1 \times 10^{-5}$ and $r = -0.84$, $df = 199$, $p < 1 \times 10^{-5}$ respectively).

We also find that these subjects display increasing controllability with age, for both mean average controllability (Pearson’s correlation coefficient $r = 0.20$, $df = 199$, $p = 5 \times 10^{-3}$) and mean modal controllability ($r = 0.16$, $df = 199$, $p = 4 \times 10^{-2}$). Synchronizability decreases with age: $r = -0.27$, $df = 199$, $p = 1 \times 10^{-4}$; and sex, brain volume, handedness and head motion have been controlled for. These results are consistent with our findings in the main text, although the p -values are larger as expected for this smaller sample size. There is a similar emergence of ‘super-controllers’ where brain regions with higher average and modal controllability, are also increasing in their controllability with age more than regions with low controllability. Regions that display increasing average controllability with age are positively correlated with their average controllability values: $r = 0.60$, $df = 233$, $p < 1 \times 10^{-5}$, just as regions that display increasing modal controllability with age are also positively correlated with their modal controllability values: $r = 0.38$, $df = 233$, $p < 1 \times 10^{-5}$. Lastly, the stable controllers in the subcortical region again show a negative correlation between the mean average controllability in those regions, and the subject’s IQ (Spearman correlation coefficient $\rho = -0.19$, $df = 233$, $p = 8 \times 10^{-3}$, controlling for age, sex, brain volume, handedness and head motion). Together, these findings match well with the results we obtain in the main text, and rule out head motion as a confounding factor for our conclusions.

Volume-normalized streamline connectivity

In the main text we use the raw number of streamline counts between brain regions as a measure of connectivity in our networks. Aware that larger regions are likely to have more streamlines that begin and end in them, we normalize each streamline count by the the total volume of the node pair [65]. This results in brain networks with much smaller weights (average strength of 0.011) as compared to the unnormalized networks (average strength of 19). When repeating our analysis on these normalized networks, in order to obtain controllability metrics that can be reasonably compared with those from the unnormalized networks, the internal normalization of $1 + \xi_0(A)$ has to be modified accordingly (where $\xi_0(A)$ is the largest singular value of the network adjacency matrix \mathbf{A} ; see Methods). For consistency of analysis, we choose a new normalization of $f + \xi_0(A)$, where $f = 0.011/19$ — the ratio between the average strengths of the normalized to unnormalized networks respectively.

Here we find that the 190 adults still display a positive correlation between whole-brain average and modal controllabilities (Pearson’s correlation coefficient $r = 0.67$, $df = 189$, $p < 1 \times 10^{-5}$), and synchronizability is negatively correlated with both mean average and modal controllabilities ($r = -0.49$, $df = 189$, $p < 1 \times 10^{-5}$ and $r = -0.62$, $df = 189$, $p < 1 \times 10^{-5}$ respectively). In the entire youth sample from ages 8 to 22, we again see that mean average controllability and mean modal controllability are both positively correlated with age: Pearson’s correlation coefficient $r = 0.28$, $df = 881$, $p < 1 \times 10^{-5}$ and $r = 0.24$, $df = 881$, $p < 1 \times 10^{-5}$ respectively. Synchronizability shows an extremely strong negative correlation with age: Pearson’s correlation coefficient $r = -0.49$, $df = 881$, $p < 1 \times 10^{-5}$. These results are controlled for sex, brain volume, handedness and head motion, and replicate well our findings for the unnormalized streamline connectivity.

On the regional level, we still see the presence of ‘super-controllers’ where brain regions with higher average and modal controllability are also increasing in their controllability with age more than the regions with low controllability. Regions that display increasing average controllability with age are positively correlated with their average controllability values: $r = 0.60$, $df = 233$, $p < 1 \times 10^{-5}$, just as regions that display increasing modal controllability with age are also positively correlated with their modal controllability values: $r = 0.48$, $df = 233$, $p < 1 \times 10^{-5}$. Lastly, the stable controllers in the subcortical region again show a negative correlation between the mean average controllability in those regions, and the subject’s cognitive performance (Spearman correlation coefficient $\rho = -0.067$, $df = 233$, $p = 5 \times 10^{-2}$, controlling for age, sex, brain volume, handedness and head motion). Together, these findings are consistent with the

results we obtain using unnormalized streamlines.

Different parcellation scale

The analysis in the main text relies on brain networks that have been constructed on regions assigned from the Lausanne atlas at the scale of 234 regions [46]. Here we repeat our analysis on networks constructed at a finer scale of 463 brain regions in this atlas. As in the earlier sections, we find that the 190 adults still display a positive correlation between whole-brain average and modal controllabilities (Pearson’s correlation coefficient $r = 0.85$, $df = 189$, $p < 1 \times 10^{-5}$), and synchronizability is negatively correlated with both mean average and modal controllabilities ($r = -0.81$, $df = 189$, $p < 1 \times 10^{-5}$ and $r = -0.74$, $df = 189$, $p < 1 \times 10^{-5}$ respectively). In the entire youth sample from ages 8 to 22, we also see that mean average controllability and mean modal controllability are both positively correlated with age: Pearson’s correlation coefficient $r = 0.28$, $df = 881$, $p < 1 \times 10^{-5}$ and $r = 0.19$, $df = 881$, $p < 1 \times 10^{-5}$ respectively. Synchronizability also decreases with age: $r = -0.36$, $df = 881$, $p < 1 \times 10^{-5}$, where we control for sex, brain volume, handedness and head motion. These results all replicate our findings at the 234-region scale well.

On the regional level, there is again the presence of ‘super-controllers’ where brain regions with higher average and modal controllability are also increasing more in their controllability with age. Regions that display increasing average controllability with age are positively correlated with their average controllability values: $r = 0.35$, $df = 233$, $p < 1 \times 10^{-5}$, just as regions that display increasing modal controllability with age are also positively correlated with their modal controllability values: $r = 0.27$, $df = 233$, $p < 1 \times 10^{-5}$. In this parcellation, the stable controllers in the subcortical region show no significant correlation between the mean average controllability in those regions and the subject’s cognitive performance (Spearman correlation $p = 0.71$), after controlling for age, sex, brain volume, handedness and head motion, suggesting that the finer parcellation masks the global drivers of individual differences in cognitive performance.

Probabilistic tractography

We used a ball and two sticks multi-compartment fiber model to fit the DTI data using the FSL bedpostx algorithm [66], which utilizes Markov chain Monte Carlo sampling to estimate uncertainty of fiber orientations at each voxel. For probabilistic tractography, we generated subject-specific seed volumes at the intersection of 234 dilated gray matter regions and the FreeSurfer

GM-WM boundary [67]. We ran FSL probtrackx [68], initiating 1000 probabilistic samples in each GM-WM boundary voxel identified in the 234 seed regions. Otherwise, we used default tracking parameters (a step-length of 0.5mm, 2000 steps maximum, curvature threshold of 0.02). We retained 878 subjects from the original sample, which passed the quality control measures for probabilistic tractography.

Networks were constructed where edge weights were equal to the number of probabilistic streamlines connecting each region pair [69]. As the resulting matrices have many more weak connections, thresholding of the lowest weights was done to obtain matrices of equivalent density (17%) to the deterministically obtained matrices. Normalization for each subject by their total network strength was also performed, and for simplicity we report the statistics for the whole youth sample. We find that mean average controllability and mean modal con-

trollability remain positively correlated (Pearson's correlation coefficient $r = 0.83$, $df = 877$, $p < 1 \times 10^{-5}$), and remain both negatively correlated with global synchronizability ($r = -0.90$, $df = 877$, $p < 1 \times 10^{-5}$ and $r = -0.83$, $df = 877$, $p < 1 \times 10^{-5}$, respectively). The trends with age remain robust: mean average controllability increases with age (Pearson's correlation coefficient $r = 0.33$, $df = 877$, $p < 1 \times 10^{-5}$) as does mean modal controllability ($r = 0.25$, $df = 877$, $p < 1 \times 10^{-5}$). Synchronizability decreases with age: $r = -0.32$, $df = 877$, $p < 1 \times 10^{-5}$, where we control for sex, brain volume, handedness and head motion.

The above results demonstrate consistency with findings obtained from deterministic tractography. Still, it will be important in future to determine a data-driven method for which to threshold the probabilistic tractography matrix, and better understand the role of these weak connections in controllability and synchronizability.